Making optical vortices with computer-generated holograms

Alicia V. Carpentier,[a] Humberto Michinel, and José R. Salgueiro
Área de Óptica, Facultade de Ciencias de Ourense, Universidade de Vigo, As Lagoas s/n, Ourense, ES-32004 Spain

David Olivieri
Departamento de Linguaxes e Sistemas Informáticos, Universidade de Vigo, As Lagoas s/n, Ourense, ES-32004 Spain

(Received 22 February 2007; accepted 16 June 2008)

An optical vortex is a screw dislocation in a light field that carries quantized orbital angular momentum and, due to cancellations of the twisting along the propagation axis, experiences zero intensity at its center. When viewed in a perpendicular plane along the propagation axis, the vortex appears as a dark region in the center surrounded by a bright concentric ring of light. We give detailed instructions for generating optical vortices and optical vortex structures by computer-generated holograms and describe various methods for manipulating the resulting structures. © *2008 American Association of Physics Teachers.*
[DOI: 10.1119/1.2955792]

I. INTRODUCTION

The phase of a light beam can be twisted like a corkscrew around its axis of propagation. If the light wave is represented by complex numbers of the form $Ae^{i\Phi}$, where A is the amplitude of the field and Φ is the phase of the wave front, the twisting is described by a helical phase distribution $\Phi = m\theta$ proportional to the azimuthal angle of a cylindrical coordinate system (r, θ, z), where z is the propagation direction of the wave train.

Because of this twisting, the light wave along the z-axis cancels out because the value of the angular coordinate θ is not well defined at $r=0$, giving rise to a phase singularity[1] where the amplitude vanishes. On a flat surface this light beam will look like a bright ring with a dark hole in its center around which the phase rotates. Due to an analogous phenomena in fluids, this light beam is called an *optical vortex* (see Fig. 1).

To assure the continuity of the field at $\theta=2\pi$, there exists an integer number m, which indicates the number of phase windings around the dark spot. This number is the *topological charge* of the vortex, because it is conserved during propagation. The physical meaning of m corresponds to the velocity of the phase rotation around the singularity, which may be positive (for counterclockwise rotation) or negative (for clockwise rotation). The definition of m is given by the z-component of the angular momentum L_z. For light beams the value of L_z per photon is given by

$$L_z = -i\hbar\frac{\partial\Phi}{\partial\theta} = -i\hbar m, \tag{1}$$

where $\hbar$ is Planck's constant divided by 2π. From Eq. (1) it is evident that the continuity condition at $\theta=2\pi$ implies the quantization of the angular momentum. The value of L_z indicates that there is a rotation of the momentum vector $\vec{p}$ around the dark hole as the beam propagates. This analogy with the velocity fields of fluids suggests that the wave front dislocation observed in light beams should be called an optical vortex.

In recent years several important applications of optical vortices have been developed. For example, the absence of the gradient force in the central hole can be used to make optical tweezers that can trap neutral particulates,[2] which receive the angular momentum associated with the rotation of the phase.[3] In nonlinear optics, waveguiding can be achieved inside the central hole.[4,5] In astronomy the singularity can be used to block the light from a bright star to increase the contrast of astronomical observations using optical vortex coronagraphs,[6] which are useful for the search of extrasolar planets. Applications in quantum information employing quantized properties of the angular momentum of vortex light beams have also been proposed.[7] Vortices are topological objects, which are important in many branches of physics such as fluid mechanics, superconductivity, Bose–Einstein condensates,[8] and superfluidity.[9] As we will show, the agreement between theory and experiment is remarkable for linear optics, and thus it provides a well characterized system for the study of such phenomena. This visual verification between theoretical and experimental results provides an added way of gaining intuition about the underlying equations and theory. For this reason, we believe that it is desirable to teach the basic laboratory techniques required to produce and manipulate optical vortices in the undergraduate physics curriculum.

The structure of the paper is as follows: In Sec. II we explain how to fabricate computer-generated holograms,[10,11] which can be used to make optical vortices. References 12–14 have described how such low-cost computer hologram experiments can be constructed. We build on this work and show how the generated holograms can be used to study several modern phenomena related with optical vortices. In Sec. III we describe the necessary elements for experimentally creating and manipulating optical beams with several vortices of topological charge $m=1$. In Sec. IV we describe using the same setup how to obtain structures with a central vortex of charge m surrounded by single-charged vortices.[15] Finally, we show how to precisely rotate the vortex lattices,[16] which is of great utility for the optical manipulation of trapped particulates.[17]

II. DESIGN OF THE HOLOGRAPHIC MASK

Optical vortices can appear spontaneously or can be created in one of several ways, such as by the manipulation of the laser cavity,[18] by employing mode converters,[19] or by a

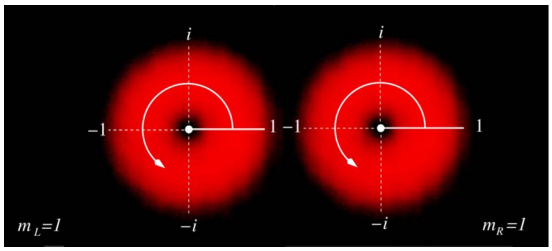

Fig. 1. Two beams with the same charge propagating in parallel directions. The origin of the phase is arbitrary with respect to the horizontal axis. In this configuration the left side of the right beam and the right part of the left beam have opposite phases.

simple technique that uses computer-generated holograms.[20,21] It has been shown in several classic papers how computer-generated holograms can be designed.[11–14] We will show how to use computer-generated holograms to produce optical vortices with optical equipment found in many undergraduate laboratories.

Our aim is to imprint a phase $e^{im\theta}$ in a Gaussian beam. Thus, we will make computer-generated holograms formed by the interference of a reference tilted plane wave $\psi_1=e^{ikx}$ (where k is the spatial frequency indicating the tilting angle of the wave) and an object wave $\psi_2=e^{im\theta}$, which carries the singular phase. When this hologram is illuminated by a beam containing the reference wave (in our experiment we will use a Gaussian beam from a laser), the object is reconstructed and the vortex appears in the output beam.

We generate a computer-generated holographic mask by painting an interference pattern proportional to the function,

$$H=|\psi_1+\psi_2|^2=|e^{ikx}+e^{im\theta}|^2=2[1+\cos(kx-m\theta)], \quad (2)$$

where $\theta=\tan^{-1}(y/x)$ is the polar coordinate. In Figs. 2(a)–2(f) we show plots of H for $m=1$ to $m=6$. When one of these holographic patterns is illuminated with a Gaussian beam $\psi_G=e^{-r^2/w^2}$ of width w, the resulting far-field Fraunhofer diffraction pattern is proportional to the Fourier transform $\mathcal{F}$ of the product $\psi_G H$ of the input function and the

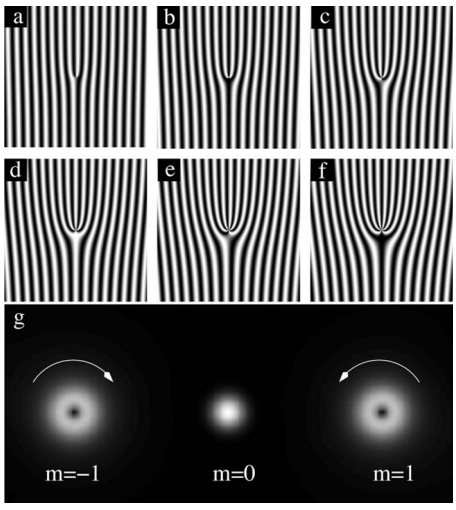

Fig. 2. (a)–(f) Different plots of $H=|\psi_1+\psi_2|^2$ from Eq. (2) for $m=1$ to $m=6$, respectively. (g) Contour plot of the function I from Eq. (3) corresponding to illuminating an $m=1$ computer-generated holograms with a Gaussian beam.

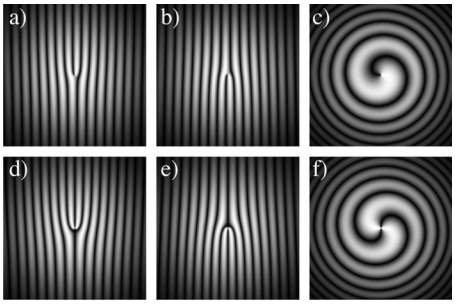

Fig. 3. Interference patterns of beams carrying topological charge m and different reference waves ψ. In (a) and (b) $m=1$ and $m=-1$, respectively, and ψ is a tilted beam with planar phase. In (c) $m=-1$ and ψ has a spherical phase. (d), (e), and (f) correspond to the same cases as the upper row for $m=2$ and $m=-2$, respectively.

hologram transmission function H. Thus, the irradiance in a plane far from the computer generated holograms is given by

$$I=\mathcal{F}[\psi_G H]=\mathcal{F}[e^{-(r/w)^2}|e^{ik_x x}+e^{im\theta}|^2], \quad (3)$$

where k_x is the x-component of the wave vector of the tilted wave. The result can be calculated with standard mathematical software and is plotted in Fig. 2(g) for $m=1$. As can be seen in Fig. 2(g), the Fourier transform of $\psi_G H$ produces a central Gaussian beam (diffraction order $n=0$) and two adjacent beams corresponding to $n=1$ and $n=-1$ carrying the phase singularities $m=1$ and $m=-1$, respectively. The intensity pattern shown in Fig. 2(g) is the same for the two vortices. However, the phase distribution rotates in opposite senses. For $m=1$ rotation is counterclockwise and for $m=-1$ it is clockwise. The result can be explained by taking into account that the Gaussian beam includes the plane wave ψ_1 used to register the hologram, and thus it can be used to reconstruct the object beam ψ_2 (the azimuthal phase).

To check the value of m for the beams in Fig. 2(g) we calculate numerically the interference of beams with $m=\pm 1$ with a plane wave. The results are shown in Fig. 3, where we show patterns corresponding to the interference of a beam with $m=\pm 1$ with a tilted plane wave [Figs. 3(a) and 3(b), respectively]. The interference between a beam with $m=1$ and a spherical wave is shown in Fig. 3(c). In Figs. 3(d) and 3(e), respectively, we show the pattern due to the interference between beams with $m=\pm 2$ with a plane wave and in Fig. 3(f) a beam with $m=2$ with a spherical wave.

III. FABRICATION OF THE HOLOGRAM

The holographic masks that are used to produce optical vortices are fabricated in a two-step process. First, the computer-generated interference patterns of Figs. 2(a)–2(f) are printed. Next, these images are transferred to a transparent photographic film using an analog camera. Because this process is an important step in creating desired optical vortices, we give the details of this two-step process.

Each of our computer-generated interference patterns consists of approximately 40 dark fringes, with an interline separation equal to the widths of the fringes. Because we wanted to reduce this pattern to an area of 0.5 cm^2, we had a line density of 16 lines/mm, and each linewidth was approximately 60 μm. Although these densities can be obtained with high-end digital laser printers (with >2400 dpi), we found that high contrast and high definition images can be obtained

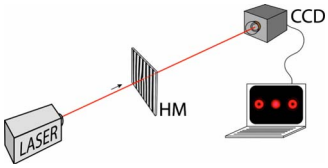

Fig. 4. Sketch of the generation of optical vortices by a computer-generated hologram. A laser beam illuminates the HM creating a diffraction pattern that can be observed on a white screen or with a CCD camera.

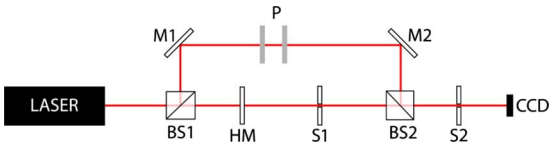

Fig. 6. Experimental setup: LASER: 1 mW He–Ne laser with $\lambda = 632.8$ nm; BS1 and BS2: beam splitters; HM: computer-generated holographic mask; S1: adjustable slit or diaphragm; M1 and M2: mirrors; P: polarizers; S2: adjustable slit for detecting $m=1$ charged optical vortices (optional); CCD: camera for imaging the interference pattern of both beams.

by taking photographs of the original interference patterns, printed on white paper, using an analog camera with black and white film. Laser printers with a spatial resolution of 1200 dpi would not be able to produce such line spacings without significant quantization error.

Because the resolution of the holographic mask is a key step in obtaining high quality vortices, we make several recommendations. When taking the photograph with the analog camera, high contrast may be obtained by slightly overexposing the film, thereby increasing the shutter time contrary to that indicated by the photometer. In practice, we took several photographs with different durations and then selected the resulting pictures optimized for contrast and resolution.

The film development process we used is standard for black and white photography and is that indicated by the film manufacturer instructions. In brief we introduce the film into a developing liquid (we employed Agfa Rodinal), perform a water rinse, and fix the image with a fixing bath using Agefix. The duration of each process varies depending on the film manufacturer. The final film contrast can be increased during the development process by increasing the temperature of the developer bath.

IV. EXPERIMENTING WITH OPTICAL VORTICES

Once the holographic mask has been made, a laser beam is passed through it, and vortices may be observed at each order (peaks) of the resulting diffraction pattern. A sketch of the experiment is depicted in Fig. 4. The result of the experiment is illustrated in Fig. 5 where the diffraction pattern obtained using a holographic mask of charge $m=2$ can be observed. We see two interesting properties of the resulting diffraction pattern: all diffraction orders have optical vortices nested within them, and the topological charge of each vortex is given by nm, where n represents the diffraction order and m the charge of the mask; the rotation of the phase is of opposite sign on each side of the diffraction maximum.

The value of the topological charge of optical vortices may be directly observed from the interference patterns between the vortex beam and a reference beam. Figure 6 depicts the experimental arrangement for creating this interference pattern. Both the vortex and reference beams must be coherent for creating interference fringes. As seen in Fig. 6, coherence is easily accomplished by dividing the original beam with a beam splitter. A vortex is created by the holographic mask, and the other beam is used for detection.

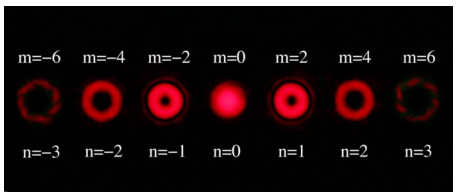

Fig. 5. Resulting diffraction pattern from the traversal of a He–Ne laser through a computer-generated holographic mask of topological charge $m=2$.

In Fig. 6 a 1 mW He–Ne laser with wavelength $\lambda = 632.8$ nm is split into two beams by the beam splitter BS1. The reference beam traces out the path from mirrors M1 through M2 and continues toward the second beam splitter BS2. The other beam traverses the holographic mask (HM), forming a diffraction pattern. The correct diffracted order is separated by the adjustable slit or diaphragm S.

The separation between the two beam splitters in Fig. 6 depends on the number of lines per centimeter of the holographic mask (the separation is 60 cm for the holographic mask described in Sec. III). Also the propagation distance should be sufficiently long so that the diffracted orders are well separated to provide individual selection with an adjustable slit or diaphragm, the position of the mirrors should make the difference between the reference and vortex beam paths small without exceeding the coherent length of the laser, and the mirrors should be mounted in tilting supports for an adequate alignment.

Another important caveat of Fig. 6 concerns the CCD imaging system that we used to record the interference patterns of vortices in real time. Because specialized CCD cameras that are sensitive to the wavelength of a He–Ne laser are expensive, we used a modified webcam by eliminating the focusing lens. This solution was cost effective, conveniently interfaced to our laboratory computer. Because the beams directly illuminate the CCD sensor, care must be taken for lasers exceeding 1 mW. For higher incident beam power it is advisable to attenuate the beam intensity to avoid saturation of the CCD sensor.

With the experimental arrangement of Fig. 6 different interference patterns may be created depending on the curvature of the reference beam. If the reference beam is a plane wave, then a characteristic fork pattern is obtained as in Fig. 7(a). The excellent agreement between the experimental results of Fig. 7 and the analytical plot of Fig. 3(a) is clearly observed. If the reference beam is spherically focused, then a pattern with m spiral arms results, as shown in Fig. 7(b) for $m=1$. For this case the numerical calculation of Fig. 3(c) also shows satisfying agreement between the theoretical and experimental results.

As an added motivation for doing experiments with optical vortices, analogous phenomena that have recently been observed in quantum liquids may be studied. One such effect is the superfluid Kelvin–Helmholtz instability,[22,23] which describes the appearance of a quantized number of vortices in the contact zone of two superfluids moving with different

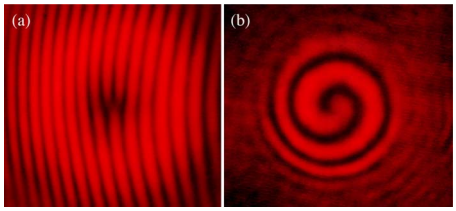

Fig. 7. Experimental interference patterns of a $m=-1$ charged vortex and (a) a tilted plane wave, and (b) a spherical wave. These results should be compared with the analytical patterns of Fig. 3.

velocities. The usual Kelvin–Helmholtz instability gives the typical cat-eye pattern in the boundary between two usual fluids moving with different velocities or in the same fluid in the presence of a velocity shear. For a superfluid the characteristic pattern evolves into an array of quantized vortices. This effect was first pointed out by Feynman in the 1950s (Ref. 24) and was recently observed in ^{3}He.[25] We stress the analogy between the superfluid Kelvin–Helmholtz instability and the formation of arrays of vortices at the boundary of two optical beams with different angular momenta. If we take into account the hydrodynamic interpretation of the wave equations of laser propagation,[26] the velocity of the fluid is proportional to the gradient of the phase. Thus, when the two beams with different m are superposed, the situation is equivalent to the existence of a velocity shear in the boundary between them. Such similarities in the observed phenomena of optical vortices are suggestive of the behavior witnessed in the contact region between the two superfluids.[27,28]

The superfluid Kelvin–Helmholtz instability can be modeled using lasers by a slight modification of our experimental arrangement to produce two copropagating light vortex beams. The idea of this experiment is to illustrate the effect of destructive interference. Given that the phase of the vortex is of the form $e^{im\theta}$, there will be m points where the phase of the ring and a plane wave have a phase difference of π, resulting in destructive interference and a dark spot in the zone where the amplitudes of the ring and the plane wave are opposite. This property can be explained by calculating the

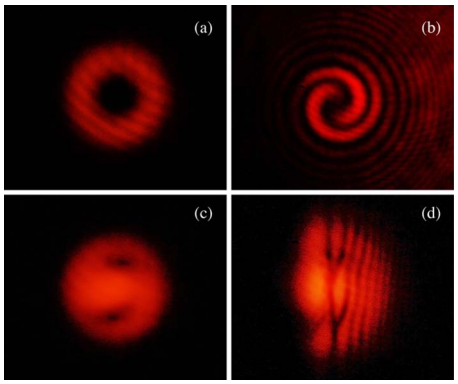

Fig. 8. (a) An optical vortex with topological charge $m=2$. (b) The resulting interference pattern of the optical vortex and a tilted spherical wave relative to the propagation direction. (c) Decomposition of the vortex into two vortices when the initial vortex is made to copropagate with a Gaussian beam. (d) Interference pattern of the two optical vortices with a tilted plane wave. These results should be compared with Fig. 3.

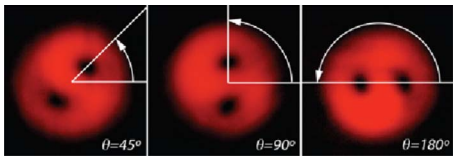

Fig. 9. Rotation control of two single charged vortices induced by varying the phase of the reference beam.

interference pattern of a constant plane wave $\Psi_p=1$ and a vortex $\Psi_v=e^{im\theta}$. The intensity pattern that is produced is described by

$$|\Psi|^2=|1+e^{im\theta}|^2=2[1+\cos m\theta]. \tag{4}$$

Destructive interference takes place if $\cos m\theta=-1$, which yields zeros at $m\theta=\pi+2n\pi$, with $n=0,\ldots,m-1$, and thereby forming m dark spots at the vertices of a regular polygon of m sides. This phenomenon can be reproduced with light by using two beams, one a Gaussian (which is the direct output of a He–Ne laser and plays the role of the plane wave) centered on the dark region of another coaxial beam carrying a vortex of charge m. In the contact region between the beams, the interference will give the same result as Eq. (4), and thus the resulting pattern will be m single charged defects, each one located in the vertex of a regular polygon of m sides, centered with both beams (see Figs. 8–10).

We can use the same experimental arrangement for creating vortices as in Fig. 6 to produce two copropagating beams by carefully adjusting the tilt angle of the mirrors so that the reference beam fits inside of the central dark region of the vortex. To obtain well defined patterns, optimal contrast of the interference pattern is sought for similar intensities of the Gaussian beam and the vortex in the superposition region. Two polarizers are used to regulate the intensity of the reference beam. The resulting pattern is recorded by a CCD camera for a given propagation length. An example of the registered images for the copropagation of a Gaussian beam and an optical vortex of topological charge $m=2$ is shown in Fig. 8. In Fig. 8(a) we observe the intensity distribution of a vortex with charge $m=2$. In Fig. 8(b) the interference pattern of the optical vortex with a spherical wave can be seen, showing two spiral arms, which confirm the value of the topological charge. The decomposition into two single-charged vortices, obtained when the $m=2$ vortex copropagates with a Gaussian beam, is shown in Fig. 8(c). An extra

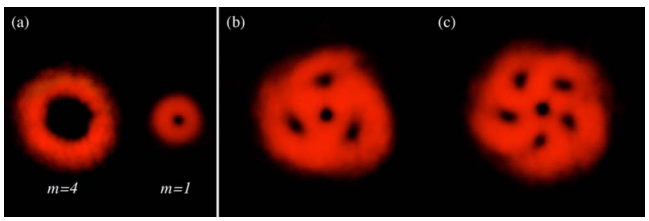

Fig. 10. Composition of two different optical vortices. (a) Vortices of topological charge $m=4$ and $m=1$. (b) Composition of vortices of topological charge $m=4$ and $m=-1$. (c) Composition of vortices of topological charge $m=4$ and $m=1$. The results in (b) and (c) are lattices formed by a vortex of charge $m=-1$ and $m=1$ in the center and three (or five) single-charged vortices around the periphery.

tilted plane wave is added in Fig. 8(d) to verify that the two dark spots observed in Fig. 8(c) correspond to vortices with charge $m=1$.

We mounted all of the optical components on the same vibration isolated table. We used a He–Ne laser because it is common in undergraduate laboratories and has the advantage that the beam can be seen without effort. All other elements of the experiment are readily purchased.

There are several practical recommendations that we suggest for obtaining good experimental results and improving the quality of the observed optical vortices. Together with ensuring that the film mask has a minimum resolution, of at least 10% of the linewidth, (or 6 μm, which corresponds to a film resolution of approximately 100 lines/mm), it is important that the light source is homogeneous both across and perpendicular to the holographic diffraction film. We found that possible polarization or intensity instabilities of the laser can be avoided by operating the laser some time before performing the experiment. The beam was spatially filtered by focusing the beam through a pinhole. We also suggest that students decompose vortices of charge $m=3$ or $m=4$ instead of vortices of charges $m=2$ or $m=1$, because alignment issues are not as critical.

V. VARIATIONS ON THE EXPERIMENT

Once the two vortex structures have been achieved by the superposition of two beams with different momenta, interesting effects can be studied by rotating the resulting vortex structure. Because the position of a single-charged vortex in the light distribution depends on the relative phase between the beams that generated the structure, an additional phase difference must be introduced between the two beams by introducing a tiltable glass plate in the path of the reference beam. In this way we can produce a variation in the phase due to the change in path length for different tilt angles. The vortex array will rotate 360° when $m\lambda=d$, where m is the topological charge of the initial optical vortex (equivalent to the number of single-charged vortices of the lattice), λ is the laser wavelength, and d is the variation of the path length. The resulting rotation can be imaged with a CCD. This effect could be used, for example, to control the rotation and position of particulates in trapping experiments.[17] Figure 9 demonstrates the rotation control of a vortex array formed by two vortices. We have created vortex arrays with vortices of charges $m=1$ through $m=6$. The case $m=1$ produces an off-axis optical vortex that rotates around the center of the beam.

Another interesting variation of this experiment is to observe additive properties of the optical vortices. This effect can be explained as follows: As described, the copropagation is achieved by putting one beam in the zero intensity zone of the other. In the overlap region between the two beams a number of single charged vortices will appear. The total number of vortices surrounding the central hole will be the sum of the initial topological charges. In Fig. 10 we have reproduced this effect using beams with charges $m=4$ and $m=\pm 1$ [see Fig. 10(a)]. We proceed to insert the single-charged vortex into the zero intensity region of the $m=4$ beam; the results are shown in Figs. 10(b) and 10(c) for charges of opposite and equal signs, respectively. Figure 10 demonstrates that the resulting number of vortices in the corona is given by the sum of the input topological charges, and the central singularity remains with charge $m=\pm 1$.

ACKNOWLEDGMENTS

This work was supported by Ministerio de Educación y Ciencia, Spain (Project Nos. FIS2004-02466, BFM2003-02832, network FIS2004-20188-E), Xunta de Galicia (Project No. PGIDIT04TIC383001PR), and MEC Ramón y Cajal Contract (JRS).

[a]Electronic mail: avcarpentier@uvigo.es

[1] J. F. Nye and M. V. Berry, "Dislocations in wave trains," Proc. R. Soc. London, Ser. A **336**, 165–190 (1974).

[2] K. T. Gahagan and G. A. Swartzlander, Jr., "Optical vortex trapping of particles," Opt. Lett. **21**, 827–829 (1996).

[3] N. B. Simpson, K. Dholakia, L. Allen, and M. J. Padgett, "Mechanical equivalence of spin and orbital angular momentum of light: An optical spanner," Opt. Lett. **22**, 52–54 (1997).

[4] A. H. Carlsson, J. N. Malmberg, D. Anderson, M. Lisak, E. A. Ostrovskaya, T. J. Alexander, and Y. S. Kivshar, "Linear and nonlinear waveguides induced by optical vortex solitons," Opt. Lett. **25**, 660–662 (2000).

[5] J. R. Salgueiro, A. H. Carlsson, E. Ostrovskaya, and Y. Kivshar, "Second-harmonic generation in vortex-induced waveguides," Opt. Lett. **29**, 593–595 (2004).

[6] G. Foo, D. M. Palacios, and G. A. Swartzlander, Jr., "Optical vortex coronagraph," Opt. Lett. **30**, 3308–3310 (2005).

[7] A. Mair, A. Vaziri, G. Welhs, and A. Zeilinger, "Entanglement of the orbital angular momentum states of photons," Nature (London) **412**, 313–316 (2001).

[8] M. R. Matthews, B. P. Anderson, P. C. Haljan, D. S. Hall, C. E. Wieman, and E. A. Cornell, "Vortices in a Bose-Einstein condensate," Phys. Rev. Lett. **83**, 2498–2501 (1999).

[9] G. W. Rayfield and F. Reif, "Quantized vortex rings in superfluid helium," Phys. Rev. A **136**, A1194–A1208 (1964).

[10] C. López-Mariscal and J. C. Gutiérrez-Vega, "The generation of nondiffracting beams using inexpensive computer-generated holograms," Am. J. Phys. **75**, 36–42 (2007).

[11] The Amateur Scientist, "Homemade hologram," Sci. Am. (Int. Ed.) **216**, 122–129 (1967).

[12] T. Seymour, "Computer simulated holography and computer generated holograms," Am. J. Phys. **64**, 472–478 (1995).

[13] A. G. Porter and S. George, "An elementary introduction to practical holography," Am. J. Phys. **43**, 954–959 (1975).

[14] J. S. Marsh and R. C. Smith, "Computer holograms with a desk-top calculator," Am. J. Phys. **44**, 774–777 (1976).

[15] I. D. Maleev and G. A. Swartzlander, Jr., "Composite optical vortices," J. Opt. Soc. Am. B **20**, 1169–1176 (2003).

[16] M. P. MacDonald, K. Volke-Sepulveda, L. Paterson, J. Arlt, W. Sibbett, and K. Dholakia, "Resolving interference patterns for the rotation of optically trapped particles," Opt. Commun. **201**, 21–28 (2002).

[17] D. G. Grier and Y. Roichman, "Holographic optical trapping," Appl. Opt. **45**, 880–887 (2006).

[18] M. Brambilla, F. Battipede, L. A. Lugiato, V. Penna, F. Prati, C. Tamm, and C. O. Weiss, "Transverse patterns. 1. Phase singularity crystals," Phys. Rev. A **43**, 5090–5113 (1991).

[19] M. W. Beijersbergen, L. Allen, H. E. I. O. van der Veen, and J. P. Woeman, "Astigmatic laser mode converters and transfer of orbital angular momentum," Opt. Commun. **96**, 123–132 (1996).

[20] N. R. Heckenberg, R. McDuff, C. P. Smith, and A. G. White, "Generation of optical-phase singularities by computer-generated holograms," Opt. Lett. **17**, 221–223 (1992).

[21] P. Coullet, L. Gill, and F. Rocca, "Optical vortices," Opt. Commun. **73**, 403–408 (1989).

[22] G. E. Volovik, "On the Kelvin-Helmholtz instability in superfluids," JETP Lett. **75**, 418–422 (2002).

[23] S. E. Korshunov, "Analog of Kelvin-Helmholtz instability on a free surface of a superfluid liquid," JETP Lett. **75**, 423–425 (2002).

[24] R. P. Feynman, "Atomic theory of the two-fluid model of liquid helium," Phys. Rev. **94**, 262–277 (1954).

[25] R. Blaauwgeers, V. B. Eltsov, G. Eska, A. P. Finne, R. P. Haley, M. Krusius, J. J. Ruohio, L. Skrbek, and G. E. Volovik, "Shear flow and Kelvin-Helmholtz instability in superfluids," Phys. Rev. Lett. **89**,

155301-1–4 (2002); A. P. Finne, T. Araki, R. Blaauwgeers, V. B. Eltsov, N. B. Kopnin, M. Krusius, L. Skrbek, M. Tsubota, and G. E. Volovik, "An intrinsic velocity-independent criterion for superfluid turbulence," Nature (London) **424**, 1022–1025 (2003).
[26]M. Vaupel, K. Staliunas, and C. O. Weiss, "Hydrodynamic phenomena in laser physics: Modes with flow and vortices behind an obstacle in an optical channel," Phys. Rev. A **54**, 880–892 (1996).
[27]M. P. Alonso and H. Michinel, "Superfluidlike motion of vortices in light condensates," Phys. Rev. Lett. **94**, 093901-1–4 (2005).
[28]C. Nore, M. E. Brachet, and S. Fauve, "Numerical study of hydrodynamics using the nonlinear schrodinger-equation," Physica D **65**, 154–162 (1993); R. Y. Chiao, T. H. Hansson, J. M. Leinaas, and S. Viefers, "Two-dimensional 'photon fluid:' Effective photon-photon interaction and physical realizations," J. Phys. B **37**, S81–S89 (2004).

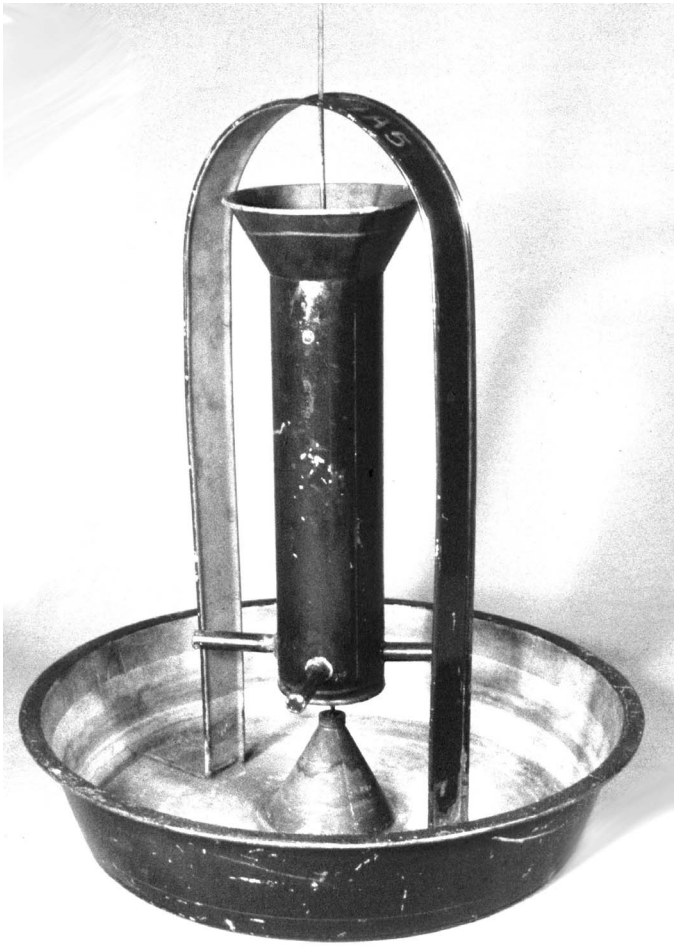

Barker's Mill. The demonstration apparatus is variously called Segner's Reaction Turbine, Parent's Mill, the Scotch Turbine, the Hydraulic Tourniquet or Barker's Mill. It was probably first invented in 1760 by Andreas Segner using Hero's steam reaction turbine as a model. Water from above pours into the funnel at the top of the central rotor that pivots freely about its axis. Projecting from the bottom of the rotor are two pipes, each closed at the end, but with a rearward-facing hole. Water spouts out of these holes, making the rotor spin. This demonstration is at Miami University in Oxford, Ohio. (Photograph and Notes by Thomas B. Greenslade, Jr., Kenyon College)